Gas-phase characterization of silicon nanoclusters produced by laser pyrolysis of silane

Markus Ehbrecht and Friedrich Huisken*
Max-Planck-Institut für Strömungsforschung, Bunsenstrasse 10, D-37073 Göttingen, Germany
(Received 3 February 1998; revised manuscript received 12 June 1998)

Silicon clusters and nanocrystals containing up to several thousand atoms per cluster have been generated by pulsed CO_2-laser-induced decomposition of SiH_4 in a flow reactor. By introducing a conical nozzle into the reaction zone, the nascent clusters are extracted into a molecular beam apparatus where they are analyzed with a time-of-flight mass spectrometer. Compared to the well-established laser vaporization method, this technique is capable of producing considerably larger silicon clusters with diameters in the nanometer size regime. A time-of-flight study of the neutral silicon clusters has shown that the velocity of the particles strongly depends on their size. This feature enables one, by introducing a chopper into the cluster beam, to considerably reduce the size distribution and to perform experiments with quasi-size-selected *neutral* clusters. An investigation of the fragmentation behavior of the ionized silicon clusters as a function of the fluence of the ionizing ArF excimer laser reveals that intermediate-size Si_n clusters ($n=22-100$) fragment by fission, yielding Si_6^+ -Si_{11}^+, while nanometric silicon clusters evaporate single Si^+ and Si_2^+ ions if the fluence of the ionizing laser is large enough. At the same time, multiply charged nanoclusters are observed. The probability of multiple ionization scales with the size of the nanoclusters. [S0163-1829(99)15203-2]

I. INTRODUCTION

In recent years, there has been increasing interest in the synthesis and characterization of nanosized particles.[1] Due to their finite size, they often exhibit physical properties that may significantly differ from those of their bulk counterparts. Research in this direction is strongly motivated by the possibility of designing nanostructured materials that possess novel electronic, optical, magnetic, chemical, and mechanical properties. Silicon is of particular importance for the microelectronics industry, and therefore a detailed knowledge of the physical and chemical properties of silicon in its mesoscopic state between the atom and bulk matter is highly desirable.

Much work has been devoted to silicon clusters containing up to $n=100$ atoms. While the structures of small Si_n clusters with $n\leqslant 10$ are well understood,[2] the transition to the bulk phase, which is realized by the mid-sized clusters, is still subject of intensive experimental and theoretical work. Consistent with the known experimental facts, the most promising structures of clusters in the size range $n<90$ ($d<1.5$ nm) are the endohedrally self-doped fullerenes.[3–5] On the other hand, large silicon clusters, containing a few thousand atoms, are found to be monocrystalline with diamond structure,[6,7] polycrystalline[8] or amorphous. However, these nanosized particles were produced as supported species, and it should be noted that the structures of free and supported clusters may be different.

The observation of photoluminescence from porous nanostructured silicon at the beginning of this decade[9,10] has triggered an enormous increase in activity.[11–13] While the early investigations were devoted exclusively to porous silicon produced by electrochemical etching of Si wafers,[11,14] recent work is concentrating more and more on the production and characterization of silicon nanoclusters constituting zerodimensional quantum dots.[15] Important issues of current research are: what is the smallest cluster size exhibiting photoluminescence, how do the luminescence wavelength and the efficiency vary with the cluster size, and what is the role of surface passivation?

In the past, most experimental studies devoted to small Si_n clusters ($n<100$) were carried out in molecular beams using a laser vaporization source to produce the silicon clusters.[16–19] Apart from being restricted to the pulsed mode and having poor long term stability, this source has the disadvantage that the maximum cluster size is restricted to approximately $n=200$.

An alternative technique, capable of producing much larger silicon clusters, is based on the pyrolysis of silicon-containing gas phase precursors, such as silane. This technique, commonly referred to as chemical vapor deposition (CVD), can be used to produce ultrafine powders and thin films. From the many possibilities to dissociate the precursor molecules, CO_2-laser-induced decomposition of SiH_4 in a gas flow reactor has been shown to be particularly useful for the production of ultraclean silicon particles in the nanometer size range.[8,20–22] However, with typical diameters above 10 nm, the particles are too large for many applications.

To close the gap between small silicon clusters ($n<200$, $d<2$ nm) and large nanoparticles ($n>2.5\times10^4$, $d>10$ nm) and to study the intermediate sizes, we have recently developed a cluster source which combines the laser-driven CVD reactor with a supersonic expansion of the nascent clusters into a high vacuum molecular beam apparatus.[23] Indeed, it could be shown that the source is capable of producing silicon nanoclusters in the desired size regime.[24,25] In addition, it was found that the velocity of the nanoclusters correlates with their mass, enabling us to perform a size selection of the neutral clusters by introducing a slotted chopper wheel. This feature has been successfully exploited to produce thin films of silicon nanoclusters and to study their photoluminescence behavior and Raman spectroscopy as a function of cluster size.[26]

While our earlier publications[24,27] report on preliminary

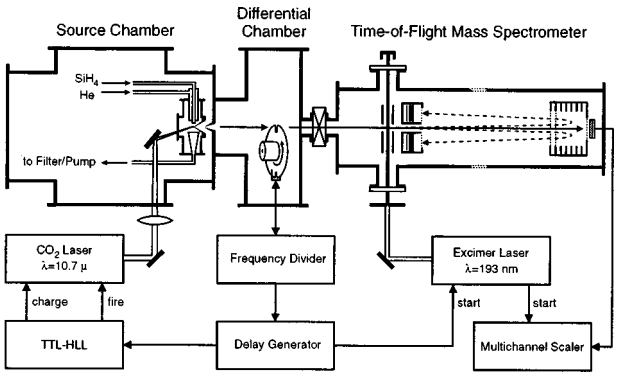

FIG. 1. Schematic view of the cluster beam apparatus.

results or focus on the Raman and photoluminescence spectroscopy of silicon nanoparticles, the present paper gives a full account to the mass spectrometric characterization of the silicon cluster beam extracted from the laser-driven CVD reactor. In presenting the experimental results, the emphasis is placed on the fragmentation of the ionized silicon clusters after interaction with 193 nm photons, the investigation of multiple ionization effects, and the determination of the actual size distributions in the different parts of the cluster pulse. With the help of a molecular-beam chopper introduced into the cluster beam, the velocities of the various cluster sizes are determined. It is shown that the same chopper can be used to select a narrow size distribution and to perform experiments with quasi-size-selected silicon nanoclusters. In contrast to the widely used laser vaporization sources, the present cluster source can be operated continuously if a cw CO_2 laser is employed.

II. EXPERIMENTAL SETUP AND DATA ANALYSIS

The experiments have been carried out in a molecular-beam apparatus that is shown schematically in Fig. 1. The setup consists of three vacuum chambers: a source chamber containing the flow reactor, a differential chamber enhousing the chopper for size selection, and a ultrahigh-vacuum (UHV) chamber that contains the time-of-flight mass spectrometer (TOF-MS). The silicon clusters are produced in the flow reactor by pulsed CO_2 laser pyrolysis of SiH_4 as has been described in detail earlier.[23,28,29] During the course of the experiments, various reactor conditions have been tested. If not otherwise stated, the results presented in this study were obtained under the following conditions, which have been found to be particularly favorable: SiH_4 flow rate: 20 sccm; He flow rate: 1100 sccm; total pressure: 330 mbar; pulse energy of the CO_2 laser: 50 mJ; laser line: $10\mu P(30)$ (934.9 cm^{-1}). Under these conditions, the background pressures in the vacuum chambers were 3×10^{-3} mbar (source chamber), 5×10^{-5} mbar (differential chamber), and 2×10^{-7} mbar (detector chamber).

The reaction products are extracted perpendicularly to both the gas flow and the CO_2 laser beam through a conical nozzle of 0.3 mm diameter opening, merging into the reaction zone. The velocity of the SiH_4 gas flow is estimated to be at most 1 m/s (Ref. 20), i.e., three orders of magnitude lower than the velocity of the silicon clusters in the beam. It also follows that the silane molecules move less than 1 μm during the 150-ns lasting pulse of the CO_2 laser. After skimming, the silicon clusters enter a pressure-reducing differential chamber of 370 mm length, and finally they reach the UHV detector chamber where they are ionized by the radiation of an ArF excimer laser ($\lambda = 193$ nm).

The mass spectrometer can be operated as a simple Wiley and McLaren[30] TOF-MS (WMTOF-MS) or as a linear reflectron-type time-of-flight mass spectrometer (RETOF-MS). If used as an ordinary WMTOF-MS the ions are detected by a pair of microchannel plates mounted at the end of the detector chamber. High-resolution mass spectra are obtained with the RETOF-MS. In this mode, an appropriate voltage is applied to the electrostatic mirror at the end of the detector chamber. It then reflects the ions back to the ion source where they are detected by another pair of microchannel plates. These channel plates have a central hole of 6 mm diameter through which the ions, after generation in the ion source, are extracted into the field-free drift region. The entire RETOF-MS setup is identical to a construction of Neusser and co-workers and has been described in more detail in their publication.[31] The high-resolution mode of our mass spectrometer has been used to reveal the isotopic composition of small silicon clusters (Si_2-Si_{11}). Due to the existence of different isotopes, the individual cluster sizes cannot be resolved in the size regime of silicon nanoclusters, even at high instrumental resolution. Therefore, all other measurements presented here, have been carried out with the ordinary WMTOF-MS.

In contrast to earlier experiments[23,24,28] in which a digital scope (Tektronix, model TDS 520) was used to record the time-of-flight mass spectra, we are now using a multichannel analyzer (EG+G ORTEC, model T914) with a dwell time of typically 200 ns. For every detected ion, the channel corresponding to the ion arrival time is incremented by one. This technique enables us to carry out experiments at much lower fluence of the ionizing laser and to accumulate the mass spectra over several thousand laser shots. Using the average function of the digital scope, small signals are lost in the background noise if such large integration times are used. This is the result of the low sampling rate (and thus unfavorable duty cycle), which must be used if extended mass spectra are to be measured.

Before entering the TOF-MS chamber through a quartz window, the ArF excimer laser beam is shaped by a 3-mm-wide and 5-mm-high aperture. Depending on the intention, laser fluences in the range from a few $\mu J/cm^2$ up to several mJ/cm^2 have been used. In order to apply even higher fluences for ionization, the laser beam was focused by either a cylindrical or a spherical lens.

In the present study, we have exclusively used the pulsed CO_2 laser for pyrolysis. As a result, the silicon cluster beam is *pulsed*, with a repetition rate of 20 Hz. This pulsed generation has the advantage that the *neutral* silicon clusters can be separated in time (and space) according to their size. By varying the delay between the generating CO_2 laser and the ionizing excimer laser, different parts of the cluster pulse (and thus different cluster size distributions) can be investigated with the mass spectrometer.

A velocity analysis of the silicon clusters was performed by modulating the neutral cluster beam with a rotating chopper wheel mounted inside the differential chamber (see Fig.

1). The chopper disk has two diametrically opposed 1-mm-wide slits and is operated at a rotational frequency of 400 cps. Using a light barrier, a by-forty frequency divider, and a variable pulse and delay generator (SRS, DG 535), the CO_2 and excimer lasers are synchronized to the chopper. The delay generator receives a trigger at time zero ($t=0$), which is defined by the moment when one of the two chopper slits passes through the light barrier. After $T=1.25$ ms the same slit crosses the molecular-beam axis. If the CO_2 laser is fired after a delay $\tau_1<T$, silicon clusters with flight times in a narrow range around $t^-=T-\tau_1$ or velocities near $v=s^-/t^-$ will be transmitted by the chopper slit. Here s^- is the distance between the nozzle and the chopper wheel ($s^-=218$ mm). After another delay τ_2 (with respect to $t=0$), the excimer laser is fired. It follows that only particles with flight times around $t^+=\tau_2-T$ or velocities around $v=s^+/t^+$ can be ionized and analyzed with regard to their mass distribution. (The distance s^+ between chopper and ionization region is $s^+=321.5$ mm.) By choosing the appropriate time τ^- between the firing of the CO_2 laser and the moment when the particles pass through the chopper slit, it is possible to select a small portion from the entire cluster pulse. Mass and velocity distributions of the silicon clusters within this selected portion may then be determined by measuring the mass spectra at different times t^+.

In order to determine the velocity distribution belonging to the neutral precursor of a specific (ionic) silicon cluster size Si_n^+, we proceed as follows. At fixed phase t_i^- between CO_2 laser and chopper, mass spectra are measured for different delays t^+ between excimer laser and chopper, covering the entire cluster pulse transmitted by the chopper in small steps of $\Delta t^+=10$ μs. If the intensities measured for each cluster size n are now plotted as a function of t^+ the time-of-flight distribution $I_{n,t_i^-}(t^+)$ of the neutral precursors of cluster size n, transmitted by the chopper at time t_i^-, is obtained. This procedure is repeated for different t_i^- (also in steps of 10 μs) so that the entire pulse produced by the cluster source is probed. Hence, the sum over all distributions

$$I_n(t^+)=\sum_i I_{n,t_i^-}(t^+) \tag{1}$$

yields the time-of-flight distribution of the neutral precursors of Si_n^+ present in the *entire* cluster pulse. Finally, the time-of-flight distribution (1) is converted to a velocity distribution $I_n(v)$.

Since the kinetic energy T_0 of large neutral clusters is of the same order of magnitude as the energy T_{ion} that they receive in the ion source, T_0 must not be neglected. Therefore, the simple relation $t\sim\sqrt{m}$ between the time of flight of the ions in the mass spectrometer and their mass is not fulfilled anymore. To perform an accurate mass calibration of the TOF spectra, the initial velocity of the neutral clusters has to be known. Then the mass calibration of the TOF spectra can be performed numerically using the proper geometric and electrostatic parameters as well as the velocity of the neutral silicon clusters. The measured ion time-of-flight distributions are converted into mass spectra according to the formula

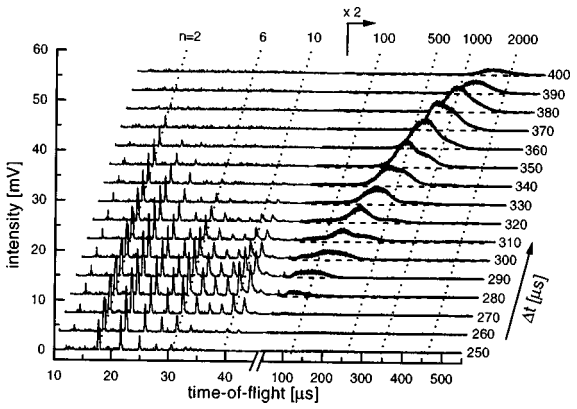

FIG. 2. TOF mass spectra of silicon clusters measured without chopper for different delays Δt between the CO_2 laser and excimer laser.

$$I(m)=\frac{I(t)\Delta t}{\Delta m}, \tag{2}$$

where $I(t)$ and $I(m)$ are the intensities in the TOF and mass spectra, respectively, and Δt and Δm the corresponding channel widths in the time and mass domains. Δm is determined numerically for each channel, taking into account the proper relation between the time of flight and mass. Size distributions (in terms of the number n of atoms) are proportional to the mass distributions since $dm/dn=\text{const}$.

III. RESULTS

A. Overview

The early experiments were carried out without chopper in the beam. First, we analyzed the temporal variation of the composition of the silicon cluster pulse extracted from the flow reactor by measuring the TOF mass spectra at different delays Δt between the firing of the CO_2 laser and the firing of the excimer laser. A typical set of TOF mass spectra obtained in this way is shown in Fig. 2. For this measurement, the fluence of the ArF excimer laser beam in the ionization region was adjusted to 21 mJ/cm^2. The cluster sizes n, which correspond to the various ion flight times are given in the top of the figure.

The first spectrum ($\Delta t=250$ μs) shows Si_n^+ cluster peaks up to $n=7$ and no signal in the region of larger masses. At larger delay ($\Delta t=280$ μs), a broad peak appears at flight times above 50 μs. This broad structure gains in intensity and shifts to larger flight times (or masses) as the delay is further increased. For example, at a delay of $\Delta t=380$ μs, the silicon cluster distribution is centered around $n=1000$, a cluster size that corresponds to a particle diameter of $d=3.4$ nm.

From the overview spectra shown in Fig. 2, we may extract the following results: (1) with the present technique we are able to produce silicon clusters in the nanosize regime, (2) the arrival time at the ionization region correlates with the size of the particles (i.e., larger particles arrive at later times than smaller ones). In addition (3), it was found that the finer details of the mass spectra were strongly dependent on the fluence of the excimer laser fluence. This shows that

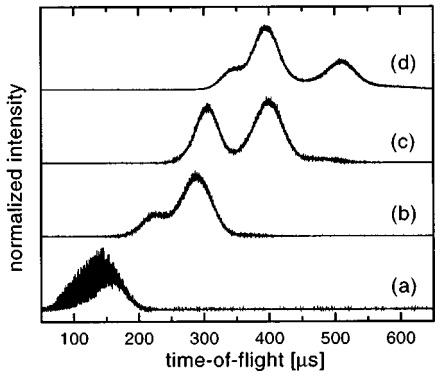

FIG. 3. Typical TOF mass spectra, recorded at different delays Δt between the CO_2 and excimer laser: (a) 280 μs, (b) 310 μs, (c) 330 μs, and (d) 350 μs. The ionization laser fluence was 2.2 mJ/cm^2 for all spectra.

fragmentation and multiple ionization are important processes that must be taken into account for a proper analysis.

The problem of multiple ionization (which mainly affects large silicon clusters) is clearly revealed in the following experiment, where we have used the molecular-beam chopper to select different narrow size distributions out of the entire silicon cluster pulse. The result of this study is depicted in Fig. 3. For each spectrum, recorded at fixed total delay $\Delta t = t^- + t^+$ between the CO_2 laser and excimer laser, the delay t^- between the CO_2 laser and chopper was adjusted to obtain maximum transmittance. The unfocused ionization laser beam had a rectangular shape of 3×5 mm^2, and the laser fluence was kept constant at 2.2 mJ/cm^2.

Spectrum (a), which has been taken in the early stage of the silicon cluster pulse, shows a uniform distribution of cluster ions centered at a flight time of 140 μs. A closer look to this spectrum reveals an onset of the signal at Si_{22}^+ and a maximum position of the size distribution around $n = 130$. In spectrum (b), the maximum has shifted to ion flight times of approximately 290 μs, corresponding to silicon clusters containing approximately 700 atoms. Furthermore, a secondary distribution is noted that appears at shorter flight times. In spectrum (c), this earlier secondary maximum increases in intensity, and in spectrum (d) even three ion distributions are clearly identified. As will be shown in Sec. III C, the secondary and tertiary peaks appearing at smaller flight times are due to doubly and triply ionized silicon clusters. From (a) to (d) the silicon cluster size continually increases and so does the probability for multiple photon absorption and thus multiple ionization. Compared to Fig. 2, the various contributions of singly and multiply ionized clusters are much better resolved, because the chopper has preselected quite narrow neutral cluster size distributions.

B. Intermediate-size silicon clusters ($n \leqslant 100$)

Figure 4 shows two TOF mass spectra taken at the early stage of the silicon cluster pulse. The delay between the CO_2 and excimer laser was set to 270 μs. Hence, the spectra were measured under conditions very similar to those of spectrum (a) in Fig. 3. The upper spectrum has been obtained with an ionizing laser fluence of 0.8 mJ/cm^2 while, for the lower spectrum, the fluence was increased to 25 mJ/cm^2.

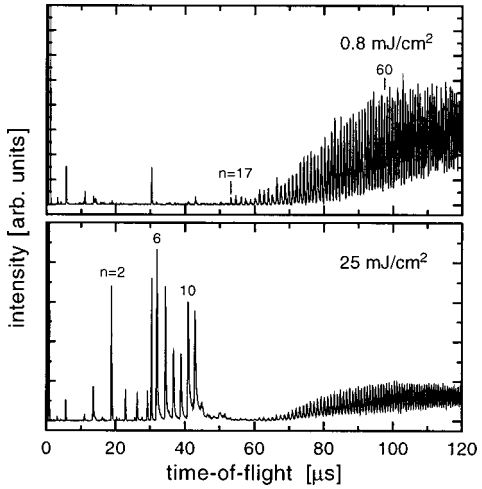

FIG. 4. TOF mass spectra recorded at the early stage of the silicon cluster pulse using different ionizing laser fluences.

The two larger peaks in the lower mass region of the upper spectrum can be assigned to He^+ and to a fragment of pump oil at $m = 152$ amu. In addition, some residual gas molecules, especially at $m = 18$ amu, are detected. The distribution of ions, which are clearly identified as silicon cluster ions, sets in at $n = 17$. This distribution has its maximum between $n = 70$ and $n = 80$. On the other hand, smaller silicon Si_n^+ clusters with $2 \leqslant n \leqslant 16$ are practically not observed (apart from some small signal for Si_{11}^+ and Si_{10}^+ and some very small signal for Si_6^+ and Si_2^+).

As can be seen in the lower spectrum of Fig. 4, some new peaks appear in the lower mass region when the ionizing laser fluence is raised to 25 mJ/cm^2. These are clearly identified as the small silicon clusters ($Si_2^+ - Si_{11}^+$). The intensity pattern and the shape of the peaks, in particular, for $Si_6^+ - Si_{11}^+$ are typical for fragmentation products that are formed by fission of the silicon clusters following multiple photon absorption. This behavior has also been observed by other investigators who used a laser vaporization source to produce their silicon clusters.[16,32,33] Since the fragmentation patterns are identical we may conclude that our clusters, that are produced by laser pyrolysis of SiH_4 in a flow reactor, must be pure silicon clusters and do not contain hydrogen.

To investigate the small silicon clusters in more detail, the mass spectrometer has been operated in its high resolution mode using the reflecting field. In this RETOF-MS mode, it was possible to resolve the isotopic composition of the smaller silicon cluster peaks ($Si_2^+ - Si_{11}^+$). Examples of these measurements are shown in Fig. 5 for $n = 3$, 6, and 10 together with the theoretical isotope distributions. The calculations are based on the natural abundances, that are 92.23% for ^{28}Si, 4.67% for ^{29}Si, and 3.10% for ^{30}Si (Ref. 34). It is seen that the measured distributions agree very well with the stick spectra of the simulation. This is another indication that the small silicon cluster ions are not contaminated with hydrogen. Otherwise one would expect higher intensities for the peaks belonging to the masses $m = 28n + 1$ or $m = 28n + 2$ amu.

C. Large silicon clusters ($n \geqslant 100$)

In order to obtain information about the origin of the different ion distributions appearing in spectra (b)–(d) of Fig. 3,

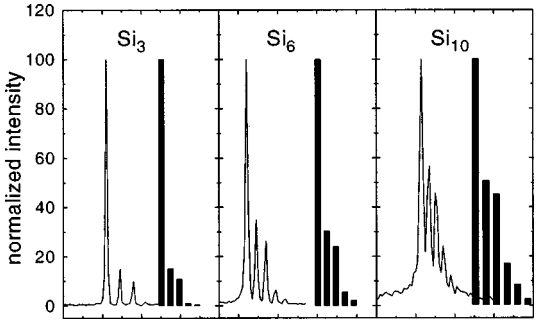

FIG. 5. Individual silicon cluster peaks, measured in the high-resolution mode, in comparison with simulations based on the natural abundances of the silicon isotopes. The separation between two adjacent lines corresponds to 1 amu.

we have studied the dependence of the mass spectra on the fluence of the excimer laser for various neutral cluster distributions. The TOF spectra have been transformed to mass spectra taking into account the proper velocities of the neutrals and the transformation factor, as described in Sec. II.

Figure 6 displays three spectra recorded at low, medium, and high laser fluence, labeled (a), (b), and (c), respectively. The delay between the CO_2 and excimer laser was adjusted to $\Delta t = t^- + t^+ = 330$ μs. Spectrum (a), recorded at the lowest fluence of 27 μJ/cm^2, is characterized by a single distribution of ions centered around 1500 silicon atoms per cluster. If the laser fluence is increased to 2.2 mJ/cm^2, a second distribution appears. It is centered at $n = 750$, and its amplitude is already larger than that of the parent distribution. It should be noted that spectrum (b) of Fig. 6 and spectrum (c) of Fig. 3 are extracted from the same measurement. The difference in the relative intensities of the two distributions as well as the increase of the noise in the region of lower masses of spectrum (a) are a consequence of the transformation into cluster size spectra (see Eq. 2). If the laser fluence is further raised, a shoulder appears in the low mass tail of the secondary distribution, as can be seen in spectrum (c) of Fig. 6.

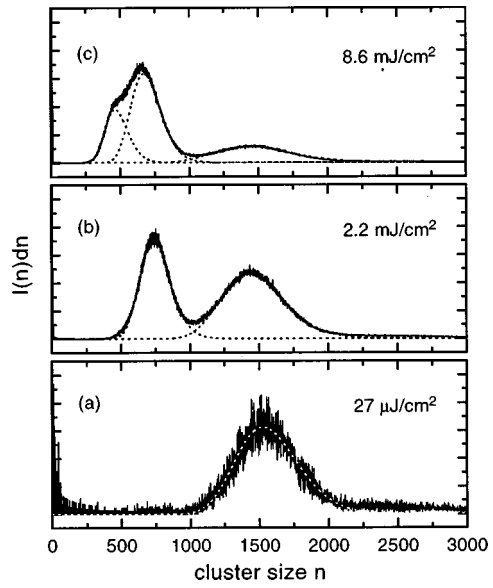

FIG. 6. Mass spectra of the same neutral cluster size distribution, measured at different fluences of the ionizing excimer laser.

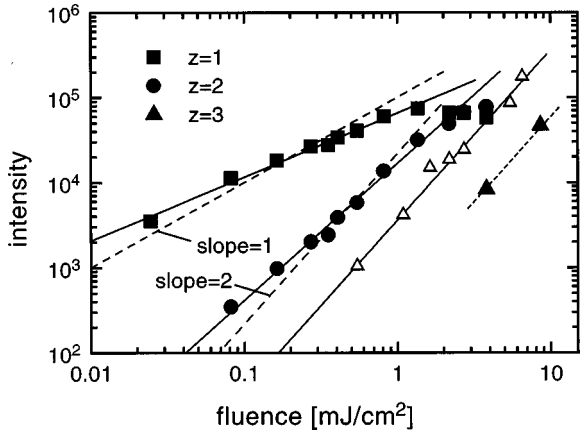

FIG. 7. Fluence dependencies of the peak areas of the spectra shown in Fig. 6 (filled symbols; $\Delta t = 330$ μs). The open triangles reveal the fluence dependence of the tertiary distribution measured for another neutral cluster size distribution containing larger species ($\Delta t = 350$ μs).

To obtain a quantitative description of the spectra, lognormal distributions have been fitted to the measurements. The fitted curves are shown in Fig. 6 as dashed lines. Comparing the maximum positions of the lognormal distributions, it seems very likely that multiply ionized silicon clusters are responsible for the distributions appearing at lower masses, for the maxima occur at $n_{max}/2$ and $n_{max}/3$, with n_{max} being the maximum position of the primary mass distribution. In order to confirm this conjecture, the area below the fitted curves has been plotted in Fig. 7 as a function of the laser fluence. The filled squares designated with $z = 1$ represent the data points obtained for the primary peaks whereas the filled circles ($z = 2$) are obtained by evaluating the secondary peaks. In the double logarithmic plot, both data sets reveal a linear increase of the intensity up to laser fluences around 2 mJ/cm^2. A least squares fit to the data yields straight lines with the slopes $p_1 = 0.8(1)$ and $p_2 = 1.6(2)$, respectively. Since the ionization potential for Si_n clusters with $n \geq 22$ is below 6 eV (Ref. 17) one ArF excimer laser photon ($h\nu = 6.4$ eV) is sufficient to ionize all larger silicon clusters. Therefore, the measured fluence dependencies, which suggest a one-photon process for the primary and a two-photon process for the secondary mass distribution, underpin the conjecture that the secondary distribution results from doubly ionized silicon clusters. The deviation from the ideal fluence dependencies with slopes 1 and 2, given by the dashed lines, is probably due to saturation effects in the ion detector. Unfortunately it is difficult to determine the exponent of the fluence dependence for the tertiary distribution from this measurement because only two data points are available (filled triangles in Fig. 7).

A closer look to the development of the tertiary distribution with the fluence of the ionization laser becomes possible if a larger mean cluster size is chosen by increasing the delay between CO_2 and excimer laser to $\Delta t = 350$ μs, the condition under which spectrum (d) of Fig. 3 was recorded. The results are given in Fig. 7 by the open triangles. A linear fit to these data points yields an exponent of the fluence dependence of $p_3 = 2.0(3)$, which is also consistent with the two data points extracted from the measurement at $\Delta t = 330$ μs (see short dashed line). It should be noted that the peak areas

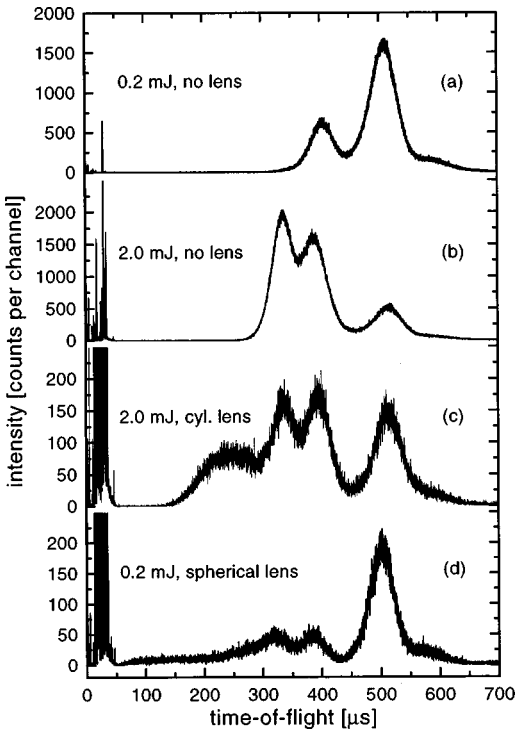

FIG. 8. TOF mass spectra of cluster ions formed under different conditions of the ionizing laser field (high mass range). The maximum of the singly ionized cluster distribution corresponds to $n = 2700$.

of the tertiary distributions are difficult to determine because of the overlap with the secondary distributions. However, the exponent of the power dependence is clearly larger than for the secondary peak, suggesting that the tertiary distribution, observed in the mass spectra at larger fluence values (and for larger cluster sizes), must be attributed to triply ionized silicon clusters.

Summarizing the fluence and size dependence studies, we state that the secondary (tertiary) distribution, occuring in the mass spectra at larger fluence of the ionization laser and/or at larger preselected neutral cluster size, has its maximum at a position corresponding to $n_{max}/2$ ($n_{max}/3$) when n_{max} is the position of the primary distribution. Furthermore, the fluence dependencies suggest a two-photon process for the secondary distribution and a three-photon process for the tertiary distribution. From these observations we conclude that the secondary mass distribution must be assigned to doubly ionized silicon clusters ($z=2$) while the tertiary distribution is formed from triply ionized nanoclusters ($z=3$). It is found that the probability and thus the cross section for multiple ionization depends strongly on the cluster size, as is evidenced by Fig. 3.

To study the behavior of silicon nanoclusters in laser fields of even larger fluence, different lenses have been used to focus the excimer laser radiation. Figure 8 shows the TOF spectra of cluster ions produced with and without a focusing lens at different laser pulse energies. The upper two spectra, designated as (a) and (b), have been taken at 0.2 and 2.0 mJ/pulse without the focusing lens. These pulse energies correspond to fluence values of 0.54 and 5.4 mJ/cm^2, respectively. The chopper has been adjusted so as to transmit a neutral silicon cluster distribution with an average cluster size of $n \approx 2700$. Whereas in spectrum (a) only singly and doubly ionized silicon clusters are observed, spectrum (b) is dominated by triply ionized species.

If the fluence is further increased (by a factor of approximately 10), by focusing the laser beam with a cylindrical lens (200 mm focal length) to a laser sheet oriented perpendicularly to the cluster beam, a broad unstructured distribution appears in the low mass tail of the triply ionized cluster distribution [spectrum (c)]. This broad distribution cannot be explained by multiple ionization since it does not show the typical pattern which should be characterized by a continually decreasing peak separation since the peak positions t_{max} have to follow the $1/\sqrt{z}$ law as the number z of charges is increased. In particular, the minimum at $t = 300$ μs is not compatible with silicon clusters having four or five positive charges. Instead, the broad distribution must be caused by fragmentation of larger clusters after absorption of more than three photons. The smallest ionic fragments in this distribution have size-to-charge ratios around $n/z \approx 200$. For energetical reasons, however, singly ionized clusters will be dominant.

The bottom spectrum of Fig. 8 has been obtained with a spherical lens (200 mm focal length) producing very high fluence in a small ionization volume. With an estimated laser beam waist of 0.2 mm, the calculated fluence is approximately 200 mJ/cm^2. Due to the small volume, the intensity of the various ionized cluster peaks is rather low [as is already the case in spectrum (c)]. Nevertheless, ions with flight times down to 60 μs are clearly observed. This indicates that the ionized clusters form ionic fragments as small as Si_{22}^+. Since the inferior beam quality of the excimer laser did not allow ideal focusing the actual focus was embedded in a larger volume with much lower fluence, which gave rise to a relatively strong contribution of singly ionized Si clusters.

Now we want to address the question of whether, in the TOF-region below 50 μs, the same fragmentation pattern is observed as if medium-size silicon clusters are ionized. This situation has been discussed along with Fig. 4. In Fig. 9 an expanded view of the low mass region of the spectra already presented in Fig. 8 is shown. Note that for each spectrum a different vertical scale is used (also compared to Fig. 8), in order to highlight the interesting features. The vertical dashed lines denote the positions of Si^+, Si_4^+, and Si_{10}^+. The positions of the other small silicon cluster ions are indicated in the bottom spectrum.

Spectrum (a), recorded at the lowest fluence, is characterized by rather low signal. The dominant peaks are attributed to He^+, to ionic fragments of the silane molecule, and to a strong contribution from pump oil fragments at 29.5 μs. As far as small silicon clusters are concerned, only a small peak is observed for the dimer; but its intensity is less than 2% of the intensity of the nanoparticles (see Fig. 8). In spectrum (b) the silicon dimer peak has become considerably larger. The corresponding count rate is of the same order of magnitude as that observed for the multiply ionized nanoclusters (Fig. 8). All other peaks appearing in the spectrum are assigned to residual gas molecules and do not belong to silicon cluster ions. In spectrum (c) silicon clusters with $n = 1-4$ are clearly identified, while larger clusters with $n \geq 5$ are not important. In particular, silicon cluster

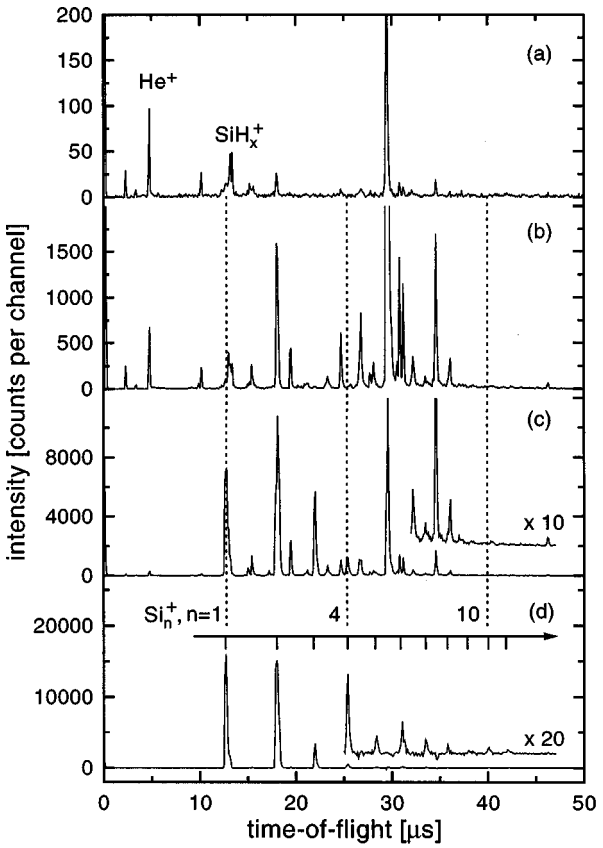

FIG. 9. Enlarged view of low mass range of the TOF spectra shown in Fig. 8.

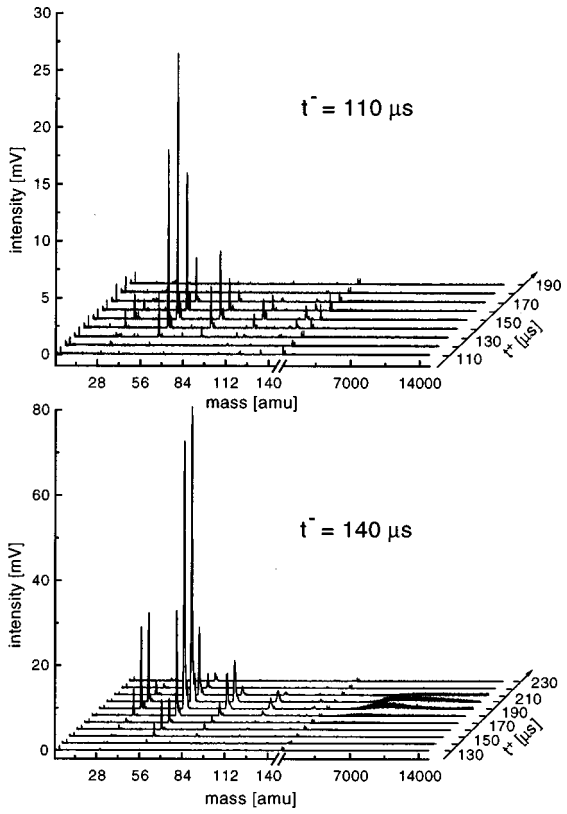

FIG. 10. Two series of mass spectra measured for different delays between chopper and CO_2 laser, probing the early part ($t^- = 110\ \mu s$) and a later part ($t^- = 140\ \mu s$) of the cluster pulse.

ions with $n=10$ and $n=11$, which are magic numbers if medium-sized ($n=22-100$) clusters are fragmented, are practically not observed. The absence of these cluster sizes becomes clearly evident in the enlarged inset of panel (c). Spectrum (d), which has been measured with the highest fluence, shows two intense mass peaks for $n=1$ and $n=2$. The larger cluster peaks are significantly weaker but, in the enlarged portion of the spectrum, they can be clearly seen up to $n=11$. In order to reveal these peaks even more clearly, we have subtracted in spectrum (d) the residual gas spectrum (background spectrum) that was recorded without firing the CO_2 laser. Although the $n=6$ peak is slightly larger than the $n=5$ peak the characteristic fragmentation pattern, as displayed in Fig. 4, cannot be observed.

As far as the fragmentation of large silicon clusters is concerned, the results of the fluence dependence study revealed by Figs. 8 and 9 may be summarized as follows. If the fluence of the ionizing laser reaches values so that multiple ionization becomes important, the dominant fragmentation channel of silicon nanoclusters is the evaporation of positively charged silicon dimers [spectrum (b)]. At higher laser fluence, fragmentation (fission) of the nanoclusters into pieces smaller than one third of the original size, accompanied by the evaporation of silicon atoms, dimers, and trimers, competes with multiple ionization [spectrum (c)]. Finally, at very high fluence, strong fragmentation into daughter ions containing a few tens of silicon atoms is observed [spectrum (d)]. Upon absorption of additional photons during the 16-ns lasting excimer laser pulse, these products further fragment into small clusters with $n=6-11$, in agreement with the result obtained earlier (compare Fig. 4).

D. Velocity analysis

As described in Sec. II, we have performed a velocity analysis of the pulsed silicon cluster beam. For this purpose, the chopper is used to preselect, at fixed delay t^-, a small portion of the initially broad silicon cluster pulse. Then the delay t^+, after which the excimer laser is fired, is varied to analyze the transmitted pulse. Figure 10 shows two examples obtained for different delays t^- between the chopper and CO_2 laser. The upper set of mass spectra ($t^- = 110\ \mu s$) reflects the situation when the early part of the cluster pulse is probed. The delay of the excimer laser (with respect to the opening of the chopper) is varied between $t^+ = 110\ \mu s$ and $t^+ = 190\ \mu s$, but significant signal is only observed in the 40 μs interval from 130 to 170 μs. If the peak intensities for a given cluster size (for example, $n=3$ at $m=84$ amu) are plotted as a function of t^+, the time-of-flight distribution of the neutral precursor (of Si_3^+ in our example) transmitted by the chopper at $t^- = 110\ \mu s$ is obtained. This neutral TOF distribution can be easily transformed into a velocity distribution by taking into account the length s^+ of the flight path. In order to obtain the complete velocity distribution representative for the neutral precursors of Si_3^+ in the entire cluster pulse, this procedure must be repeated for all relevant delays t^-. The lower part of Fig. 10 shows another set of mass spectra measured at a delay $t^- = 140\ \mu s$. In these mass spectra, silicon cluster ions Si_n^+ in the range of n

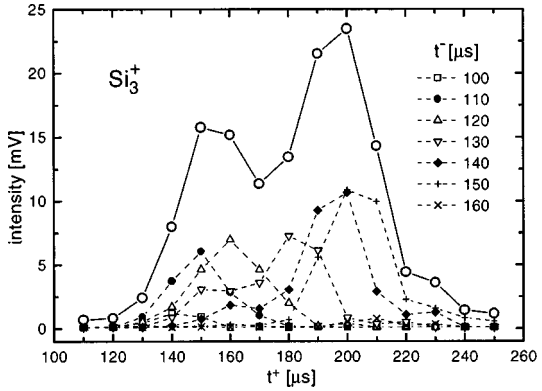

FIG. 11. Time-of-flight distributions of the neutral precursors of Si_3^+ selected from different parts of the silicon cluster pulse. The sum curve, given by the open circles, is representative for all neutral precursors present in the pulse.

$=250$ ($m=7000$ amu) are clearly visible. In addition, it is noted that the highest Si_3^+ peak ($m=84$ amu) is now observed at $t^+=200$ μs while, in the upper set of mass spectra, it occured at $t^+=150$ μs. In Fig. 11 all time-of-flight distributions of the Si_3^+ precursors, measured along the entire silicon cluster pulse in steps of 10 μs, are collected. The two distributions extracted from the data of Fig. 10 are indicated by the filled data points. The sum curve, given by the open circles, represents the overall TOF distribution of *all* neutral precursors present in the silicon cluster pulse. As will be discussed later, the peak at larger flight times ($t^+ \approx 200$ μs) results from the fragmentation of larger (and slower) clusters.

The analysis just described for Si_3^+ has been carried out for various cluster sizes up to $n=3500$. Afterwards the TOF distributions were converted into velocity distributions taking into account the proper flight path length of $s^+ = 321.5$ mm. Figure 12 displays the velocity distributions of the neutral precursors of some representative silicon cluster ions with $n=2,\ 4,\ 6$, and 10 atoms. The distributions for $n=2,\ 4$, and 6 (and the ones for $n=1,\ 3$, and 5, which are not shown) reflect a bimodal behavior. In order to obtain a quantitative description, we have fitted Gaussian distributions to the experimental data points. This results in a slow component centered around 1600 m/s and a fast contribution with its maximum at approximately 2000 m/s. While the fast contribution is assigned to fragments of medium-sized ($n=22-100$) silicon clusters the slow component is due to Si_n^+ ions evaporated from large silicon clusters. The intensity of the slow component continually decreases with increasing mass of the detected ion. For cluster sizes larger than $n=6$, the slow component is not observed anymore. The corresponding distributions can be fitted by a single Gaussian whose maximum continually shifts to smaller velocities as the cluster size is further increased. The velocity distributions of the large cluster sizes, that cannot be resolved in the TOF mass spectra, are determined in the same way: the corresponding signals measured at fixed ion flight time are plotted as a function of t^+ and then summed over all delays t^-.

The results of the velocity analysis are summarized in Fig. 13. The open circles represent the maxima of the velocity distributions while the error bars indicate their full widths at half-maximum. Figure 13 clearly shows that the velocity of

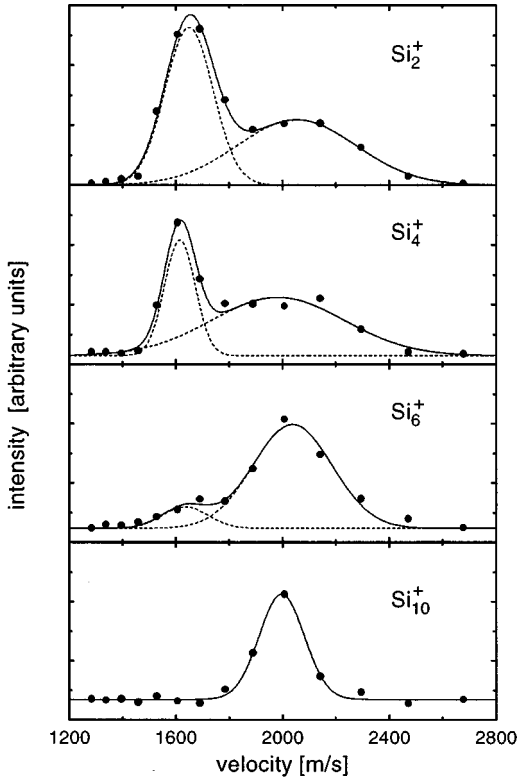

FIG. 12. Velocity distributions of the neutral precursors for some selected silicon cluster ions.

the silicon clusters extracted from the flow reactor strongly depends on their size. Small clusters containing only a few atoms are accelerated during the expansion of the gas through the nozzle to velocities around 2000 m/s. On the other hand, large silicon clusters are considerably slower. For example, the neutral precursors of $n=2500$ have velocities around $v=1400$ m/s.

Up to now we have only talked about the neutral precursors of the detected cluster ions. This is because, in the initial stage of the present study, we employed the less sensitive digital scope for taking the mass spectra. It required the use of rather high excimer laser fluence, which may have resulted in multiple ionization of the silicon nanoclusters. Since the measurements shown in Figs. 2 and 10 have been

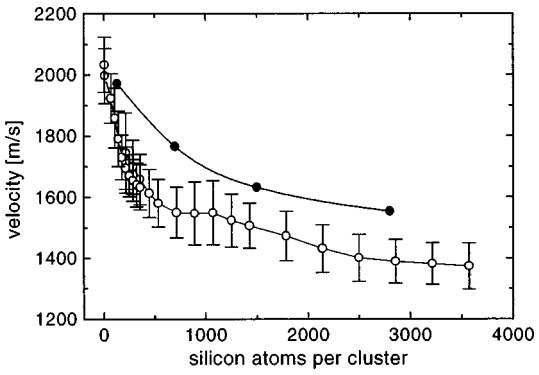

FIG. 13. Open circles: Measured velocities of the neutral precursors of the detected cluster ions of size n/z at large excimer laser fluence. Solid circles: Only singly ionized clusters are considered.

carried out under these high fluence conditions, the extracted results (Figs. 11, 12, and 13) may be affected by multiple ionization. When we used the more sensitive multichannel analyzer, which allowed us to work at lower fluences, we realized that multiple ionization indeed represents a serious complication if larger fluences are applied. Thus, it appears that the parent cluster sizes belonging to the open data points of Fig. 13 have been determined too small. Consideration of the multiple ionization effect would shift them to larger cluster sizes. In the final stage of the present study, when we were able to work with much lower excimer laser fluences, we have repeated the velocity analysis for a few cluster size distributions selected by the chopper wheel. Evaluating only the distributions of the singly ionized nanoclusters, the solid circles of Fig. 13 were obtained. Although the velocity dependence of the corrected curve is somewhat less pronounced it still shows a large variation from $v=2000$ m/s to $v=1600$ m/s for Si_n cluster sizes below $n=3000$.

IV. DISCUSSION

Although the dissociation of silane results in the production of hydrogen atoms and molecules it is found that the silicon clusters encountered in the beam do not contain hydrogen. This is inferred from the excellent agreement of the measured high-resolution RETOF mass spectra with calculations based on the natural isotope abundances of silicon. This conclusion is further supported by the close resemblance of the present mass spectra with earlier results obtained by other investigators who employed laser vaporization sources containing high-purity silicon.[16,17,32] We have also investigated the internal structure of the silicon nanoclusters using high-resolution electron microscopy (HREM). These studies, which will be the subject of a forthcoming publication,[35] revealed that the silicon nanoclusters having diameters between 3 and 10 nm are monocrystalline with the same lattice parameters as encountered in bulk *c*-Si. The absence of hydrogen can be explained by the fact that the silicon clusters are extracted from the hot region of the reaction zone, the temperature of which is estimated[20] to be 1200 K or even more. At these elevated temperatures, any chemisorption of atomic hydrogen will result in the associative desorption of hydrogen molecules.

The silicon clusters are cooled by collisions with helium atoms during the expansion and, further downstream, by evaporative cooling. Their ultimate temperature is not known. During the supersonic expansion the lighter silicon clusters are accelerated much more efficiently as a result of the collisions with the carrier gas atoms. This explains the large velocity mismatch between the light and heavy silicon clusters. The velocity is found to decrease from $v=2000$ m/s for the lightest silicon clusters to $v=1500$ m/s for the heaviest species ($n\approx 4000$). In this context it is also interesting to note that a neat supersonic beam of helium atoms expanded through a room temperature nozzle has a velocity of $v=1760$ m/s. For an assumed reaction zone temperature of 1200 K,[20] the He beam velocity is calculated to be 3500 m/s. Thus, the measured velocity of the small silicon clusters of $v=2000$ m/s can be easily rationalized.

The mass spectra measured for various delays between the pyrolyzing CO_2 laser and ionizing excimer laser reveal that the silicon cluster pulse emanating from the flow reactor is characterized by a rather large size distribution. Figures 2 and 3 show that, at constant operating conditions of the flow reactor, the cluster size may range from $n=22$ to $n>2000$. Due to the size-dependent velocity of the silicon clusters produced by the present technique, the cluster size distribution can be further narrowed by introducing a chopper into the beam and operating it with constant phase with respect to the pulsed CO_2 laser. As has been demonstrated very recently,[26] narrow size distributions with full widths at half-maximum of $\Delta d=1-1.5$ nm can be selected from the entire cluster pulse.

Although the kinetic energy of a 3-nm silicon cluster appears with $E_{\mathrm{kin}}=440$ eV rather high it should be noted that the energy per atom is only 410 meV. Thus the present cluster source is very well suited for low-energy cluster beam deposition experiments.[36] Indeed, as has been shown by Raman and luminescence studies, the silicon clusters do not fragment or coalesce if they are deposited on solid substrates.[26] In good agreement with other low-energy cluster beam deposition experiments,[37] it was found that the size of the free clusters is retained in the deposited films. This proves the usefulness of mass spectrometry of gas phase nanoparticles for characterizing thin films. However, as has been shown in the present study, care must be taken to avoid multiple ionization and fragmentation.

If a modest laser fluence of 2.2 mJ/cm^2 is applied to ionize the silicon clusters, the smaller clusters ($n\geqslant 22$) are singly ionized. In contrast, for the larger clusters, doubly and triply ionized species are observed. This behavior can be rationalized if one considers that, with growing cluster size, the absorption cross section and the ionization cross section continually increase. As a result of the Coulomb repulsion acting on the positive charges, positively charged atoms and, to an even larger extent, silicon dimers (Si_2^+) are evaporated. This effect is well manifested in Fig. 9.

In order to discuss the competition between multiple ionization and fragmentation of nanosized silicon clusters on a somewhat more quantitative level, it is useful to consider the following simple model, which has been used to describe the multiple ionization of large sodium clusters.[38] In a classical picture, the ionization potential of a large cluster can be written as the sum of the work function, W_b, and an electrostatic term describing the energy of a conducting sphere with radius r.[39] Then the energy $I(z,r)$, needed to remove an additional electron from a $(z-1)$-fold positively charged sphere, is calculated to be

$$I(z,r)=W_b+(2z-1)e^2/2r. \tag{3}$$

If the radius r is kept constant the ionization potential increases linearly with the number of charges. Assuming a typical cluster size ($n=3000$, $r=2.43$ nm) and $W_b=4.87$ eV,[17] we calculate that the ionization potential equals the energy of an ArF excimer laser photon ($E=6.42$ eV) for $z=3.12$. According to this simple picture, a single photon is sufficient to produce a threefold charged silicon cluster ion from Si_{3000}^{2+}; but at least two photons are required for the next ionization step. This result is in perfect agreement with the experimental finding that the highest ionization state is $z=3$ [see Fig. 8(b)]. Additional absorption of

excimer laser photons results in internal heating and the evaporation of small silicon cluster cations as is evidenced by Fig. 8(c) and Fig. 9(c).

Figures 11 and 12 show bimodal time-of-flight and velocity distributions for Si_n^+ with $n=1-6$. It is quite obvious that the slow component must be assigned to silicon cluster cations being evaporated from larger silicon clusters at sufficiently high laser fluence. Since this component is characterized by a mean velocity slightly above 1600 m/s it follows that the small cluster cations must have been evaporated from nanoscale silicon clusters with $n \geqslant 1000$. Our experiments show that the largest cation produced in this way is Si_6^+.

The evaporation behavior of nanosized silicon clusters is completely different from what is observed for the small silicon clusters between $n=22$ and $n=150$. If a higher laser fluence is applied to ionize these smaller species, they fragment by evaporating small positively charged Si_n^+ clusters with $n=6-11$ (see Fig. 4). The same result has been obtained earlier by Zhang *et al.*[32] One possible explanation of this would be that the Si_n clusters with $n<150$ are built from smaller subunits containing $n=6-11$ atoms. While these subunits probably have quite stable cage structures they are bonded to each other rather loosely. This interpretation is also in accord with the spectroscopic study of Rinnen and Mandich[40] who observed surprisingly identical spectra for the entire size range between $n=18$ and $n=41$. The conclusion from this experiment was that the silicon clusters share one or more common structural entities.[40]

High-resolution transmission electron microscopy has revealed that the silicon nanoparticles, collected in the cluster beam on TEM grids with holey carbon films, are characterized by a perfect monocrystalline structure with the same lattice parameters as encountered for bulk silicon.[35] In contrast, the nanoclusters collected in the flow reactor are much larger ($d>20$ nm) and mostly amorphous. This shows that the early extraction of the silicon clusters from the high pressure reaction zone is essential for obtaining crystalline nanoclusters.

V. SUMMARY

CO_2-laser-induced decomposition of silane in a flow reactor has been employed to produce silicon clusters over a very large size range. Using a conical nozzle, the nascent clusters were extracted from the reaction zone into a high vacuum molecular-beam apparatus where they were ionized by 193 nm photons and analyzed in a time-of-flight mass spectrometer. The analysis revealed that the cluster source was capable of producing Si_n^+ clusters with n varying from a few tens to several thousands. These larger silicon clusters have diameters in the range between 2 and 7 nm and are referred to as nanoclusters. Other experiments[26,35] have shown that these nanoclusters have crystalline structure, thus representing so-called *quantum dots.*

We have shown that the nanoclusters can be characterized in the gas phase using the same techniques as employed in cluster research, in particular time-of-flight mass spectrometry. However, due to their large photoabsorption cross section, care must be taken to avoid fragmentation and multiple ionization of the nanoclusters. Furthermore, we have demonstrated that the velocity of the silicon clusters ejected from the pulsed source strongly depends on their size. This property enabled us, by introducing a mechanical chopper into the cluster beam, to select different portions from the originally broad size distribution and to perform experiments with quasi-size-selected neutral clusters. This particularly attractive feature has been exploited very recently to study the photoluminescence of silicon qantum dots as a function of their size.[26]

ACKNOWLEDGMENTS

The authors would like to thank Professor H. Pauly for his continued interest and support. They are grateful to Professor H. J. Neusser for his valuable help in constructing the reflectron time-of-flight mass spectrometer. Furthermore, the help of Dr. H. Ferkel and Dr. W. Zhang in setting up the reflectron and carrying out earlier experiments is gratefully acknowledged. This work was supported by the Deutsche Forschungsgemeinschaft in the frame of its Schwerpunktprogramm *Fine Solid Particles*.

*Electronic address: fhuiske@gwdg.de

[1] See for example: *Nanostructures and Mesoscopic Systems*, edited by W. P. Kirk and M. A. Reed (Academic, New York, 1992); *Nanophase Materials: Synthesis, Properties, Applications*, edited by G. C. Hadijipanyis and R. W. Siegel (Kluwer Academic, London, 1994); *Nanomaterials: Synthesis, Properties and Applications*, edited by A. S. Edelstein and R. C. Cammarata (Institute of Physics, Bristol, U.K., 1996).

[2] E. C. Honea, A. Ogura, C. A. Murray, K. Raghavachari, W. O. Sprenger, M. F. Jarrold, and W. L. Brown, Nature (London) **366**, 42 (1993).

[3] M. F. Jarrold, U. Ray, and Y. Ijiri, Z. Phys. D **19**, 337 (1991).

[4] M. V. Ramakrishna and J. Pan, J. Chem. Phys. **101**, 8108 (1994).

[5] U. Röthlisberger, W. Andreoni, and M. Parinello, Phys. Rev. Lett. **72**, 665 (1994).

[6] H. Takagi, H. Ogawa, Y. Yamazaki, A. Ishizaki, and T. Nakagiri, Appl. Phys. Lett. **56**, 2379 (1990).

[7] S. Tamir and S. Berger, Thin Solid Films **276**, 108 (1996).

[8] Y. L. Li, Y. Liang, K.–S. Xiao, F. Zheng, and Z.–Q. Hu, Nanostruct. Mater. **5**, 1 (1995).

[9] L. T. Canham, Appl. Phys. Lett. **57**, 1046 (1990).

[10] V. Lehmann and U. Gösele, Appl. Phys. Lett. **58**, 856 (1991).

[11] Y. Kanemitsu, Phys. Rep. **263**, 1 (1995).

[12] C. Delerue, G. Allan, and M. Lanoo, Phys. Rev. B **48**, 11 024 (1993).

[13] N. A. Hill and K. B. Whaley, J. Electron. Mater. **25**, 269 (1996).

[14] D. J. Lockwood and A. G. Wang, Solid State Commun. **94**, 905 (1995).

[15] K. A. Littau, P. J. Szajowski, A. J. Muller, A. R. Kortan, and L. E. Brus, J. Phys. Chem. **97**, 1224 (1993).

[16] J. R. Heath, Y. Liu, S. C. O'Brian, Q.-L. Zhang, R. F. Curl, F. K. Tittel, and R. E. Smalley, J. Chem. Phys. **83**, 5520 (1985).

[17] K. Fuke, K. Tsukamoto, F. Misaizu, and M. Sanekata, J. Chem. Phys. **99**, 7807 (1993).

[18] A. A. Seraphin, S.-T. Ngiam, and K. D. Kolenbrander, J. Appl. Phys. **80**, 6429 (1996).

[19] P. Mélinon, P. Kéghélian, B. Prével, A. Perez, G. Guiraud, J. Lebrusq, J. Lermé, M. Pellarin, and M. Broyer, J. Chem. Phys. **107**, 10 278 (1997).

[20] J. S. Haggerty and W. R. Cannon, in *Laser-Induced Chemical*

Processes, edited by J. I. Steinfeld (Plenum, New York, 1981), pp. 165–241.
[21] W. R. Cannon, S. C. Danforth, J. H. Flint, J. S. Haggerty, and R. A. Marra, J. Am. Ceram. Soc. **65**, 324 (1982); **65**, 330 (1982).
[22] R. Fantoni, E. Borsella, S. Piccirillo, C. A. Nannetti, R. Ceccato, and S. Enzo, Appl. Surf. Sci. **43**, 308 (1989).
[23] M. Ehbrecht, H. Ferkel, V. V. Smirnov, O. M. Stelmakh, W. Zhang, and F. Huisken, Rev. Sci. Instrum. **66**, 3833 (1995).
[24] M. Ehbrecht, H. Ferkel, V. V. Smirnov, O. M. Stelmakh, W. Zhang, and F. Huisken, Surf. Rev. Lett. **3**, 807 (1996).
[25] M. Ehbrecht, H. Ferkel, and F. Huisken, Z. Phys. D **40**, 88 (1997).
[26] M. Ehbrecht, B. Kohn, F. Huisken, M. A. Laguna, and V. Paillard, Phys. Rev. B **56**, 6958 (1997).
[27] M. Ehbrecht, H. Ferkel, F. Huisken, L. Holz, Yu. N. Polivanov, V. V. Smirnov, O. M. Stelmakh, and R. Schmidt, J. Appl. Phys. **78**, 5302 (1995).
[28] M. Ehbrecht, M. Faerber, F. Rohmund, V. V. Smirnov, O. M. Stelmakh, and F. Huisken, Chem. Phys. Lett. **214**, 34 (1993).
[29] M. Ehbrecht, Ph.D. thesis, University of Göttingen, 1996; Max-Planck-Institut für Strömungsforschung, Report No. 9/96 (1996).
[30] W. C. Wiley and I. H. McLaren, Rev. Sci. Instrum. **26**, 1150 (1955).
[31] B. Ernstberger, H. Krause, A. Kiermeier, and H. J. Neusser, J. Chem. Phys. **92**, 5285 (1990).
[32] Q.-L. Zhang, Y. Liu, R. F. Curl, F. K. Tittel, and R. E. Smalley, J. Chem. Phys. **88**, 1670 (1988).
[33] M. F. Jarrold and E. C. Honea, J. Phys. Chem. **95**, 9181 (1991).
[34] *Handbook of Chemistry and Physics*, edited by D. R. Linde, 72nd ed. (CRC Press, Boca Raton, 1991).
[35] H. Hofmeister, F. Huisken, and B. Kohn (unpublished).
[36] P. Mélinon, V. Paillard, V. Dupuis, A. Perez, P. Jensen, A. Hoareau, J. P. Perez, J. Tuaillon, M. Broyer, J. L. Vialle, M. Pellarin, B. Baguenard, and J. Lerme, Int. J. Mod. Phys. B **9**, 339 (1995).
[37] V. Paillard, P. Mélinon, V. Dupuis, J. P. Perez, A. Perez, and B. Champagnon, Phys. Rev. Lett. **71**, 4170 (1993).
[38] U. Näher, H. Göhlich, T. Lange, and T. P. Martin, Phys. Rev. Lett. **68**, 3416 (1992).
[39] M. Seidl, K.-H. Meiwes-Broer, and M. Brack, J. Chem. Phys. **95**, 1295 (1991).
[40] K.-D. Rinnen and M. L. Mandich, Phys. Rev. Lett. **69**, 1823 (1992).